On the Velocity of Expanding Spherical Gas Bubbles Rising in Line in Supersaturated Hydroalcoholic Solutions: Application to Bubble Trains in Carbonated Beverages

Gérard Liger-Belair,[†] Richard Marchal,[†] Bertrand Robillard,[‡] Thierry Dambrouck,[†] Alain Maujean,[†] Michèle Vignes-Adler,[§] and Philippe Jeandet*[,†]

Laboratoire d'Œnologie, UPRES EA 2069, URVVC, Faculté des Sciences de Reims, B.P. 1039, 51687 Reims Cedex 2, France, Moët & Chandon, Laboratoire de Recherches, 6 rue Croix de Bussy, 51200 Epernay, France, and Laboratoire des Phénomènes de Transport dans les Mélanges CNRS, 4 ter route des Gardes, 92190 Meudon, France

Received May 27, 1999. In Final Form: October 7, 1999

We report in this paper measurements of the rising velocity of champagne bubbles, investigated by using a camera and a stroboscopic light. It is shown that the velocity of bubbles during ascent is intermediate between that of a rigid sphere and that of a fluid sphere free from surface-active compounds. We show that our experimental results are compatible with a model of surfactant diffusive flux toward a moving sphere, suited to the case of rising and expanding gas bubbles. The critical surface concentration of contaminants needed to completely rigidify the bubble interface may not be reached in real conditions, i.e., in a flute. The rising velocity of champagne bubbles is then compared with the velocity of bubbles in beer. Contrary to champagne bubbles, beer bubbles are found to behave hydrodynamically as rigid spheres.

1. Introduction

Since the work of Leonardo da Vinci in the early 16th century,[1] numerous researchers have investigated the rise velocity of bubbles of various sizes through various liquids. As a result, this subject has generated a huge bibliography. However, only recently, much interest was devoted to the formation and the stability of bubbles in carbonated beverages.

Bubbles in champagne wines are made of carbon dioxide, produced during alcoholic fermentation. In the closed bottle, according to Henry's law, an equilibrium is established between the wine and the headspace under the cork. When the bottle is opened, the pressure of CO_2 in the headspace falls, and the CO_2 concentration in the champagne is not in equilibrium any more with its partial pressure in the vapor phase. The liquid enters a metastable state; it becomes supersaturated with CO_2. As a result, the champagne will degas. In the case of liquids with low supersaturating ratios, such as sparkling wines, bubbles need pre-existing gas cavities to nucleate.[2,3] Gas-filled sites are generated when the liquid flows over the wall, during the filling of the flute. Details of the mechanism of gas entrapment by a liquid front advancing over a rough surface are given by Bankoff.[4] In champagne, several kinds of particles stuck on the glass wall are able to entrap gas pockets during the filling of a flute.[5,6] As a result of supersaturating, CO_2 molecules diffuse from the bulk of the liquid to the gas pocket. A bubble forms and grows from this nucleation site. When buoyancy overcomes the vertical component of the adhesive force anchoring the bubble to the cavity, the bubble detaches from its nucleation site. Then, another bubble will grow from this nucleation site and detach at the same size, and so on. As a result, bubbles are released from nucleation sites with clockwork regularity.[7,8] Regular bubble trains in a glass of champagne are therefore the result of the cycle of bubble production. Assuming a collection of pre-existing microcavity shapes and sizes on the glass wall, one can observe in the same flute and at the same time various bubble trains with various bubble formation frequencies.[8]

As concerns bubble ascent, many authors noticed the high influence of surface-active compounds on the rising velocity of bubbles.[9−11] More recently, Ybert and di Meglio[12] thoroughly examined the velocity of ascending air bubbles of fixed radius in protein solutions. They showed that the velocity of bubbles is strongly reduced compared to the velocity in pure water, because of the protein molecules adsorbed on their surface. They also provided an experimental relation between the bubble velocity and its surface concentration of protein; they used bovine serum albumin (BSA) as standard protein. Champagne wines are multicomponent hydroalcoholic systems containing in addition to alcohol many other organic compounds which may show surface activity. During their ascent toward the liquid

* To whom correspondence should be addressed: fax, 11 333 26 91 33 40; e-mail, philippe.jeandet@univ-reims.fr.

[†] Laboratoire d'Œnologie, UPRES EA 2069, URVVC, Faculté des Sciences de Reims.

[‡] Moët & Chandon, Laboratoire de Recherches.

[§] Laboratoire des Phénomènes de Transport dans les Mélanges CNRS.

(1) Fairbrother, T.; Ishikawa, I. *Leonardo lives: The Codex Leicester and Leonardo da Vinci's Legacy of Art and Science*; University of Washington Press: 1998.

(2) Dean, R. B. *J. Appl. Phys.* **1944**, *15*, 446.

(3) Bankoff, S. G. *Trans. ASME* **1957**, 735.

(4) Bankoff, S. G. *AIChE J.* **1958**, *4*, 24.

(5) Lehuédé, P.; Robillard, B. *Proceedings of the First in Vino Analytica Scienta Symposium*; Bordeaux, France, 1997.

(6) Sénée, J.; Viaux, L.; Robillard, B.; Duteurtre, B.; Vignes-Adler, M. *Food Hydrocolloids* **1998**, *12*, 217.

(7) Casey, J. A. *The Australian Grapegrower and Winemaker* **1988**, *295*, 19.

(8) Liger-Belair, G.; Marchal, R.; Robillard, B.; Vignes-Adler, M.; Maujean, A.; Jeandet, P. *Am. J. Enol. Vitic.* **1999**, *50*, 317.

(9) Levich, B. V. *Physicochemical Hydrodynamics*; Prentice Hall: Englewood Cliffs, NJ, 1962.

(10) Griffith, R. M. *Chem. Eng. Sci.* **1962**, *17*, 1057.

(11) Aybers, N. M.; Tapuccu, A. *Wärme- Stoffübertragung* **1969**, *2*, 118.

(12) Ybert, C.; di Meglio, J.-M. *Eur. Phys. J., B* **1998**, *4*, 313.

10.1021/la990653x CCC: $19.00
Published on Web 12/03/1999

Table 1. Characterization of the Investigated Liquids

liquid	alcohol content (g L^{-1})	protein content BSA (mg L^{-1})	surface tension σ (mN m^{-1})	kinematic viscosity ν (mm^2 s^{-1})	density ρ (kg L^{-1})
champagne	96.3	4.3 ± 0.5	46.8 ± 0.6	1.66 ± 0.02	0.998
beer	52.8	122 ± 2	43.5 ± 0.5	1.49 ± 0.02	1.005

surface, champagne bubbles certainly collect such surface-active compounds, which probably affect their ascending velocity. Now, most of the previous studies were conducted on single bubbles of fixed radius. The case of champagne bubbles is nevertheless quite far removed from this ideal situation. In carbonated beverages in general, and in champagne in particular, bubbles continue to expand by mass transfer when rising through the liquid, because of supersaturating. Furthermore, since bubbles are released from a few specific nucleation sites on the glass wall, bubbles rise vertically aligned and close to each other.[7,8] To the best of our knowledge, no experimental results of the ascending velocity of expanding bubbles rising in line in supersaturated surfactant solutions have been reported up to now. Bubble trains in carbonated beverages are a wonderful and common illustration of such a phenomenon. Thus, the close examination of bubbles rising in carbonated beverages may contribute to a better understanding of the adsorption kinetics on expanding spherical gas bubbles. This paper reports a study on the rising velocity of champagne and beer bubbles, based on the close examination of regular bubble trains in real conditions, i.e., in a flute.

2. Experimental Section

2.1. Materials. For these experiments, we chose standard commercial champagne wine and beer, both presenting a very typical bubbling behavior. We used a cylindrical classical crystal flute (Mariana-ARYSTAL, France) with a diameter of 4.9 cm and wall thickness of 0.8 mm. Prior to each experiment, the flute was rinsed several times using distilled water and then air-dried. The liquid surface tensions were measured with a pendant droplet apparatus (KRÜSS). Kinematic viscosities were measured with an Ubbelohde capillary viscosimeter (type 501 10/I). Protein concentrations were determined by spectrocolorimetry, using a modified Bradford procedure with bovine serum albumin (BSA) as standard protein;[13,14] results are expressed in mg/L BSA; this method gives reliable data when molecular weight of the polypeptide is higher than 3 kDa. The alcohol concentration was measured by infrared refractometry. Physical and chemical characteristics of the carbonated beverages used are given in Table 1.

2.2. Experimental Setup. A 150 mL portion of liquid was poured into the flute. To capture the motion of rising bubbles, we developed a simple but reliable method, which consists of the association of a camera and a stroboscope. The camera (Olympus OM2) used to photograph bubble trains was fitted with bellows and with a 50 mm 1:1.8 objective. The focus plane was chosen near the inner glass wall. A flash unit (SUNPAK AUTO-ZOOM 3600), synchronized with the camera diaphragm aperture, was put behind the flute. To homogenize the light, a white translucent plastic screen was placed between the flute and the flash source. To obtain photographs with a sharp resolution, a low-sensitive film (Ilford Pan F 50 ASA) was used. External light disturbances were eliminated by covering the whole system with a black sheet. Paper with graduated lines attached to the glass wall gave the scale. Photographs were enlarged 10 times. By comparing the scale given by the graduated paper stuck on the glass wall with an other one plunged into the wine, close to the inner wall, we made sure that the thickness and the curvature of the wall could not have any magnifying effect on a bubble train. On a photograph, bubble diameters and distances between successive bubble centers were measured with a ruler assuming an error of $\Delta = \pm 0.2$ mm. Therefore, real distances were measured with a standard error of $\delta = \Delta/10 = \pm 20$ μm. To have access to bubble radii, we first measured bubble diameters. Bubble radii were thus measured with a less standard deviation of $\delta_{radius} = \pm 10$ μm.

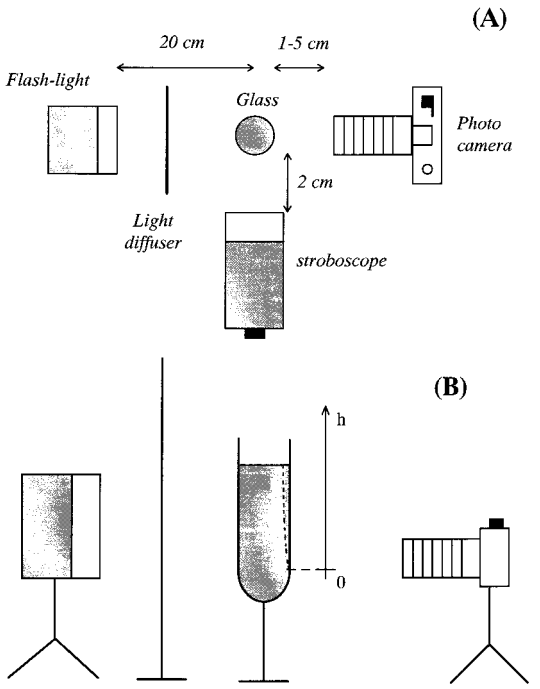

Figure 1. Experimental setup: (A) top view, (B) side view.

To show the regularity of bubble production, bubble trains were lit with the stroboscope (DIGITAL INSTRUMENT DT-2239-2), flash frequencies ranged from 1.5 to 200 Hz. At a certain frequency of strobe lighting, a regular bubble train appears "motionless", which means that the frequency f at which the stroboscope emits flashes is the same as the frequency at which the nucleation site generates bubbles. Henceforth, as we know the time interval between two successive bubbles, the photograph of each bubble train can be treated now as a succession of pictures of the same bubble, separated from the period of bubble formation $T = 1/f$. The standard error on bubble formation frequency is evaluated by observing the range of frequencies on which the bubble train appears "motionless". A value of $\delta_f \approx \pm 0.1$ Hz was found. Therefore, using the value of the frequency found with strobe lighting, it becomes possible from a single photograph to deduce the velocity of rise for a single bubble. The velocity U_n of the nth bubble in the train may be deduced from the position of the one that just precedes indexed $n + 1$ and the one that just follows indexed $n - 1$. Thus, $U_n = (h_{n+1} - h_{n-1})/2T$, where h is the traveled distance for a bubble from its nucleation site.

The experimental setup is schematized in Figure 1. To eliminate the influence of the initial liquid convection on bubble motion, observation of bubble trains (strobe lighting and photography) was conducted for 3 min at least after pouring the liquid into the flute. Experiments were performed at room temperature (20 ± 2 °C).

3. Results and Discussion

3.1. Shape Regime for Rising Champagne Bubbles. Bubbles in free rise under the influence of gravity may experience a wide range of different shape regimes (spherical, ellipsoidal, skirted, ...). The regime of bubble motion varies considerably with the following dimension-

(13) Bradford, M. M. *Anal. Biochem.* **1976,** *72*, 248.
(14) Marchal, R.; Seguin, V.; Maujean, A. *Am. J. Enol. Vitic.* **1997**, *48*, 333.

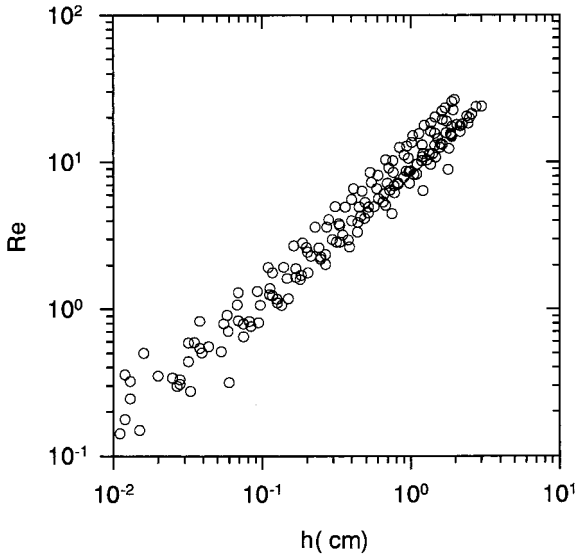

Figure 2. Reynolds number (Re) as a function of the traveled distance, *h*, for bubbles of various bubble trains.

less numbers, depending on both fluid and bubble parameters

$$\mathrm{Re} = 2\rho RU/\eta \quad \text{and} \quad M = g\eta^4/\rho\sigma^3 \tag{1}$$

Re and *M* are respectively the Reynolds and Morton numbers, with ρ and η respectively the liquid density and viscosity, σ the liquid surface tension, *g* the acceleration due to gravity, *R* the bubble radius, and *U* its velocity of rise. This Morton number depends only on the liquid properties. Champagne at 20 °C has a very low value of 7×10^{-10}. In a liquid with a low Morton number, bubbles rising at low to moderate Reynolds numbers ($\mathrm{Re} < 10^2$) will have negligible deformations[11,15] (as long as no dimple effect occurs).

We have plotted, in Figure 2, Re as a function of the traveled distance *h*, for bubbles of various bubble trains. During ascent, a champagne bubble covers a range of Re between approximately 0.1 and 50. Therefore, champagne bubbles in real conditions, i.e., in a flute, are closely approximated by spheres all along their ascent toward the liquid surface, as can be noticed on the photograph displayed in Figure 3.

3.2. Rising Velocities of Champagne Bubbles. A short examination of the typical regular bubble train presented in Figure 3 is already very instructive. It appears clearly that bubbles grow during ascent. Moreover, as the distance between two successive bubbles increases, and since bubbles are released from the nucleation site with clockwork regularity, it can be guessed that a bubble accelerates when rising through the liquid. In Figure 4, we have plotted the bubble velocity as a function of its radius, $U(R)$, during ascent for various bubble trains. $U(R)$ is superimposed with the well-known Stokes velocity

$$U_{\mathrm{ST}} = \frac{2\rho g}{9\eta} R^2 \tag{2}$$

nevertheless applicable for rigid sphere conditions and for Re lower than unity, and with the velocity derived by Levich[9] applicable for fluid spheres conditions (bubbles with a fully mobile interface) within the range of Re between 50 and 800

(15) Clift, R.; Grace, J. R.; Weber, M. E. *Bubbles, drops and particles*; Academic Press: New York, 1978.

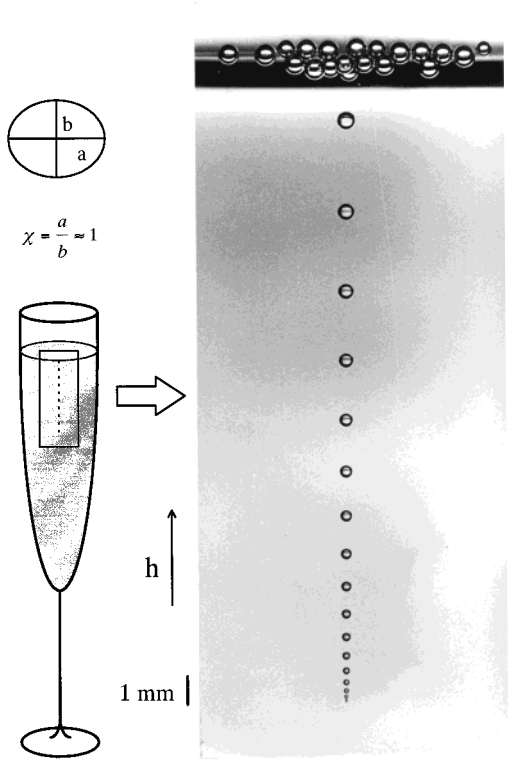

Figure 3. Photograph of a typical regular bubble train.

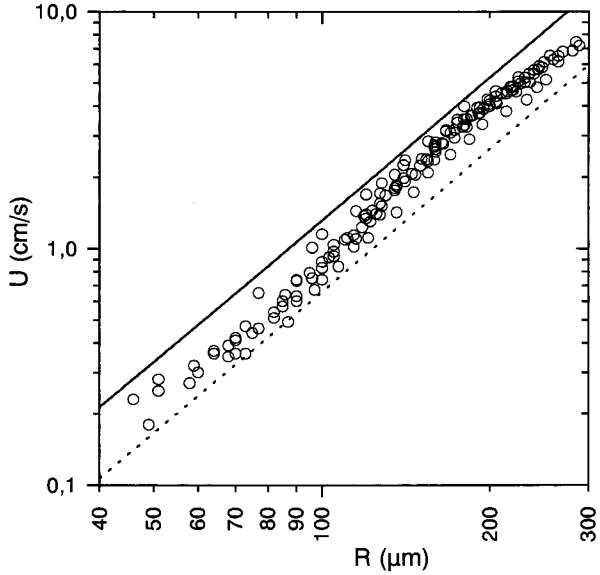

Figure 4. Experimental bubble velocities $U(R)$ (○), compared with Stokes velocity (—) and with the velocity derived by Levich (- - -).

$$U_{\mathrm{LEV}} = \frac{\rho g}{9\eta} R^2 \tag{3}$$

In terms of the power law, Figure 4 suggests a quadratic dependence with the radius for the velocity of rise. To a quite good approximation, the bubble ascent close to the glass wall can be modeled by a modification of the numerical prefactor in Stokes law

$$U(R) = \frac{2\rho g\alpha}{9\eta} R^2 \quad \text{with} \quad \alpha \approx 0.6-0.9 \tag{4}$$

Actually, because Stokes law is available only for $\mathrm{Re} < 1$, this comparison has little physical significance. It should only be used as a quick and easy way to model bubble

ascent in a glass of champagne. Maxworthy et al.[16] made a thorough examination of the rise of air bubbles in clean viscous liquids. They generated air bubbles in a various proportions of water and glycerin, which allowed them to cover a wide range of Re and M. For $M < 3.8 \times 10^{-4}$, they also found a quadratic dependence of the bubble velocity with its radius, until bubbles are slightly deformed.

Now, to better analyze hydrodynamic and physicochemical parameters that control bubble ascent, let us write the equation of motion of an expanding spherical gas bubble, rising in a low viscous fluid, as in the case of champagne bubbles. After release from its nucleation site, a bubble experiences, in addition to the buoyancy

$$F_B = \rho g \frac{4}{3} \pi R^3$$

a viscous drag force exerted by the surrounding fluid. Chakraborty and Tuteja[17] obtained theoretically that the drag force F_D exerted on a growing bubble is the same as that exerted in the absence of radial expansion. This drag force is classically expressed by

$$F_D = C_D \frac{\rho U^2}{2} \pi R^2$$

where C_D is a drag coefficient. Furthermore, because champagne bubbles are growing during ascent, they induce a displacement of the surrounding liquid which leads to an "added-mass" effect. The general expression of this added-mass force is

$$F_{AM} = \rho C_{AM} \frac{d}{dt}\left(\frac{4}{3} \pi R^3 U\right) \quad (5)$$

where C_{AM} is the added-mass coefficient. As a result, the equation of motion can be written under the form

$$\rho g \frac{4}{3} \pi R^3 - C_D \frac{\rho U^2}{2} \pi R^2 - \rho C_{AM} \frac{4}{3} \pi R^3 \left(\frac{dU}{dt} + \frac{3U}{R} \frac{dR}{dt}\right) = 0 \quad (6)$$

The volume of liquid that departs with the bubble should be about half of the bubble volume.[18,19] Otherwise, Magnaudet et al.[20] reported numerical simulations of the forces acting on a sphere embedded in accelerated flows. For flows around both a rigid sphere and a spherical bubble, their results show that the added-mass coefficient is $C_{AM} = 1/2$, whatever the Reynolds number over the range $0.1 \leq Re \leq 300$.

To compare quantitatively the added-mass term with buoyancy, we measured the ratio of F_{AM} to F_B

$$\frac{F_{AM}}{F_B} = \frac{C_{AM}}{g}\left(\frac{dU}{dt} + \frac{3Uk}{R}\right) \quad (7)$$

where k is the bubble growth rate dR/dt, pointed to be constant during ascent in a previous study of effervescence in champagne.[8]

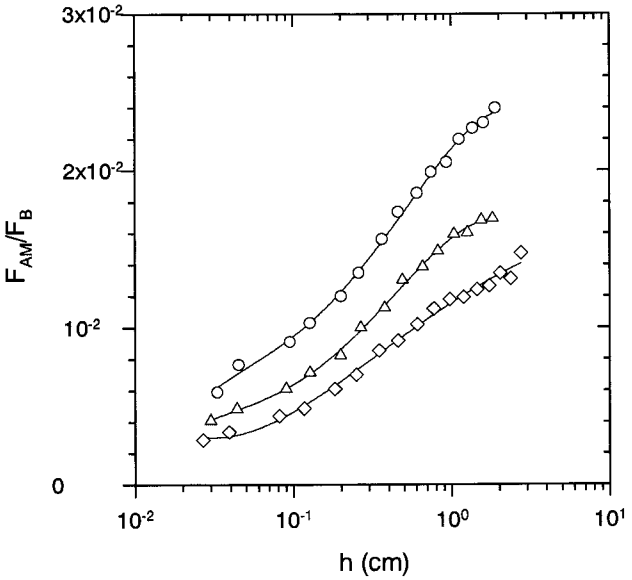

Figure 5. Ratio of the added-mass force to the buoyancy as a function of the traveled distance, h, for bubbles of three typical bubble trains: (○) $f = 25.5$ Hz; (△) $f = 20.1$ Hz; (◇) $f = 17.8$ Hz.

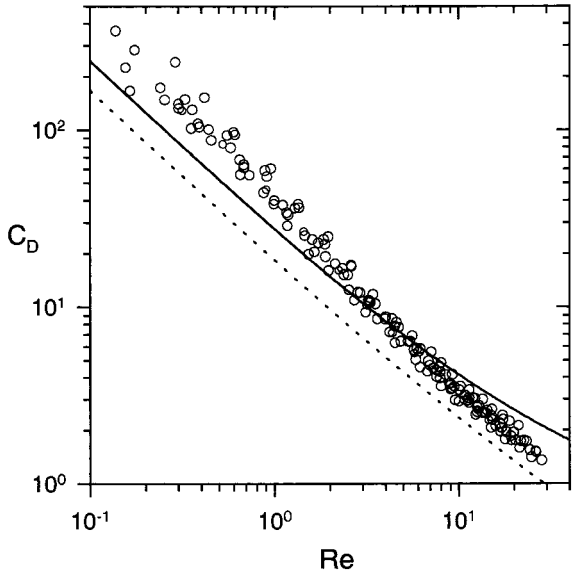

Figure 6. Drag coefficient as a function of the Reynolds number: (○) experimental results for bubbles C_D; (—) empirical relation for rigid spheres C_{RS}; (- - -) empirical relation for fluid spheres C_{FS}.

We have plotted in Figure 5 this ratio (7) as a function of the traveled distance h for three typical bubble trains. This term continuously grows during ascent, but nevertheless remains very low. The added-mass effect of a bubble approaching the free surface is only 2−3% of its buoyancy. As a result, it will be neglected afterward. Thus, the equation of motion (6) reduces itself to the classical balance between drag force and buoyancy. Now, for each bubble of a given bubble train, the experimental determination of R and U leads to the experimental determination of the drag coefficient C_D along the rise, through the expression

$$C_D = 8gR/3U^2 \quad (8)$$

We have plotted in Figure 6 experimental C_D as a function of the Reynolds number Re for various bubble trains. Many empirical or semiempirical equations have

(16) Maxworthy, T.; Gnann, C.; Kürten, M.; Durst, F. *J. Fluid Mech.* **1996**, *321*, 421.
(17) Chakraborty, B. B.; Tuteja, G. S. *Phys. Fluids A* **1993**, *5*, 1879.
(18) Milne-Thomson, L. M. *Theoretical Hydrodynamics*, 5th ed.; Macmillan: London, 1972.
(19) Naciri, A. Contribution à l'étude des forces exercées par un liquide sur une bulle de gaz: portance, masse ajoutée et interactions hydrodynamiques. Thesis, Ecole Centrale de Lyon, Lyon, France, 1992.
(20) Magnaudet, J.; Rivero, M., Fabre, J. *J. Fluid Mech.* **1995**, *284*, 97.

been proposed to approximate C_D for bubbles in free rise.[15] Our measurements are compared with two of them available in the whole range of Re covered by champagne bubbles. The first one concerns rigid spheres (applicable for bubbles covered with surfactants)

$$C_{RS} = \frac{24}{Re}(1 + 0.15Re^{0.687}) \quad (9)$$

$$Re < 800$$

The second one has been obtained for fluid spheres, i.e., bubbles with a fully mobile interface free from surface-active materials[20]

$$C_{FS} = \frac{16}{Re}(1 + 0.15Re^{0.5}) \quad (10)$$

$$Re < 50$$

C_{RS} and C_{FS} constitute the two limiting boundaries of the drag coefficient for a bubble rising in an infinite medium, at low to moderate Reynolds numbers.

Just after release from nucleation site, and below a short distance h_c on the order of a few millimeters, the experimental C_D is higher than C_{RS}. Then, above h_c, C_D progressively exhibits an intermediate value between C_{RS} and C_{FS}. To summarize:

$$h < h_c,\ C_D > C_{RS} \quad (i)$$

$$h > h_c,\ C_{RS} > C_D > C_{FS} \quad (ii)$$

These experimental observations, (i) and (ii), upon the experimental drag coefficients of champagne bubbles may be interpreted as follows:

(i) This first stage may be attributed to an inertial regime. The stationary process during which buoyancy always equilibrates drag force has not been reached yet. Furthermore, the liquid medium in which bubbles rise is not infinite. Just after release from nucleation site, bubbles rise close to the glass wall. Therefore, wall effects are certainly not negligible. Clift et al.[15] presented a complete review of the corrections to apply to bubbles rising in bounded fluids. In the case of a bubble of radius R, rising at low Re parallel to the wall of a container (available for a champagne bubble in the early moments of its ascent)

$$\frac{U}{U_\infty} \approx 1 - \frac{9}{16}\frac{R}{d} \quad (11)$$

where U_∞ is the rising velocity of the bubble in an infinite fluid, U the real velocity in the bounded fluid, and d the distance from the center of the bubble to the wall. Just after detachment from the glass wall, d is comparable with R. As a result, real rising velocities may be severely reduced in comparison with the ideal situation of an infinite medium. Therefore, for the foregoing reasons, it is not surprising that during the first moments of its life, the bubble exhibits a drag coefficient higher than C_{RS}.

(ii) There are surface-active substances in champagne likely to be adsorbed at the bubble surface, such as proteins and glycoproteins.[21−23] Such materials will certainly modify the bubble surface state during ascent and therefore the velocity of bubbles in comparison with the velocity of bubbles rising in a liquid free from surface-active compounds. Adsorption of surface-active substances affects the velocity through the Marangoni effect. The liquid flow around the bubble carries such molecules to the rear of the bubble. Consequently, a surface tension gradient appears. This gradient is responsible for a viscous shear stress on the bubble surface which decreases its velocity compared to the pure liquid case. By measuring the rising velocity of ascending air bubbles in a various proportions of BSA solution, Ybert and di Meglio[12] determined that the minimum amount of protein needed to completely rigidify the bubble interface is $\Gamma_{CR} \approx 0.5$ mg/m^2. In champagne, because the velocity of bubbles is intermediate between the one in a pure liquid and the one of a rigid sphere, we are tempted to conclude that the bubble surface is only partially rigidified during ascent.

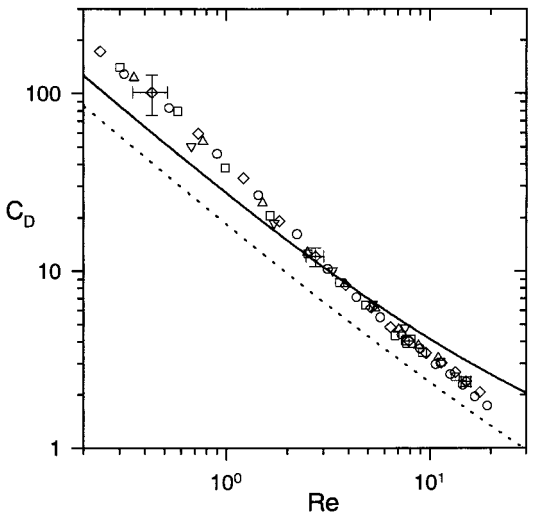

Figure 7. C_D(Re) for bubbles of a given bubble train followed while degassing: (○) $f = 22.5$ Hz; (◇) $f = 19.7$ Hz; (□) $f = 15.7$ Hz; (△) $f = 11.5$ Hz; (▽) $f = 6.6$ Hz.

However, before proceeding further with this reasoning, we must go about another problem. During ascent, bubbles are not isolated. Bubble formation frequencies may be very high, often on the order of 10−20 Hz.[8] Henceforth, bubbles rise close to each other, from less than one bubble diameter at the bottom of the train to only some bubble diameters at the top. As a result, bubbles in a train may interact with their surrounding neighbors, therefore modifying the simple balance between drag force and buoyancy, expressed by (8).

3.3. Bubble Interactions. To evaluate bubble interactions, we focus on six bubble trains that we "follow" with time, while degassing. As bubbles progressively discharge CO_2 molecules from the bulk of the liquid, the bubble formation frequency of a given nucleation site decreases with time. As a result, distances between successive bubbles of a given bubble train progressively increase. Then, if significant interactions between successive bubbles do exist, there should be a difference of drag coefficient C_D(Re), between high and low frequencies. We have plotted in Figure 7 the typical behavior observed in terms of drag coefficient, for a bubble train the frequency of which decreases with time while degassing. Variations of C_D between the different bubble formation frequencies are close to error bars, and from Re ≈ 2−4, C_D remains intermediate between C_{RS} and C_{FS}, whatever bubble formation frequencies.

(21) Brissonnet, F.; Maujean, A. *Am. J. Enol. Vitic.* **1993**, *44*, 297.
(22) Malvy, J.; Robillard, B.; Duteurtre, B. *Sci. Aliments* **1994**, *14*, 88.
(23) Marchal, R.; Bouquelet, S.; Maujean, A. *J. Agric. Food Chem.* **1996**, *44*, 1716.

Finally, if interactions between successive bubbles do exist, they are very limited (in the range of frequencies and Re covered in champagne) and hardly detectable with our experimental setup. Thus, since bubble interactions have none or only minor effects on the bubble rise, we can now reconsider rising velocities in terms of bubble surface state.

3.4. Evaluation of the Surface-Active Materials Adsorption Kinetics. During ascent, surface-active substances accumulate at the bubble interface and contribute to its rigidifying by increasing the amount of adsorbed materials.[12] However, at the same time, the bubble continuously grows as a result of supersaturating. Therefore, the area of the bubble interface increases, thus diluting the amount of the adsorbed materials. Bubbles experience two opposing effects. To evaluate the adsorption kinetics on champagne rising and growing bubbles, we retrieved results upon contaminants flux to a moving drop, obtained at low Re by Levich[9] and at large Re by Yang et al.[24] For a fluid sphere moving in a solution containing a surface-active substance, they derived the following expression

$$\frac{\mathrm{d}\Gamma}{\mathrm{d}h} = \lambda c_0 \sqrt{\frac{D}{UR}} \tag{12}$$

where Γ is the surface concentration of contaminants, h the traveled distance, D the diffusion coefficient of the surface-active compound, c_0 its concentration in the bulk, and λ a numerical factor nevertheless depending on Re. Ybert[25] reported observations of ascending air bubbles with Re $\approx 10^2$, in BSA solutions. His experimental measurements were in accordance with relation (12) for $\lambda = 0.35$.

In this model, desorption of the adsorbed materials is not supposed to occur during ascent and is therefore not taken into account.

By combining the empirical relation $U(R)$ found above (4) with (12), one finds

$$\frac{\mathrm{d}\Gamma}{\mathrm{d}h} \approx \lambda c_0 D^{1/2} \left(\frac{9\eta}{2\rho g \alpha}\right)^{1/2} R^{-3/2} \tag{13}$$

Now, since the bubble growth rate k during ascent is constant,[8] the rate of increase of the bubble radius with h becomes

$$\frac{\mathrm{d}R}{\mathrm{d}t} = \frac{\mathrm{d}R}{\mathrm{d}h}\frac{\mathrm{d}h}{\mathrm{d}t} = \frac{\mathrm{d}R}{\mathrm{d}h} U = k \tag{14}$$

i.e.

$$\frac{\mathrm{d}R}{\mathrm{d}h} = \frac{k}{U}$$

Combining (4) and (14) and performing the integration leads to

$$R = \left(R_0^3 + \frac{27\eta k}{2\rho g \alpha} h\right)^{1/3} \tag{15}$$

where R_0 is the bubble radius at detachment. Finally, by inserting the function $R(h)$ determined above in relation (13) and by performing the integration, one obtains the semiempirical dependence of Γ with h

$$\Gamma(h) = \frac{2\lambda D^{1/2} c_0}{3k}\left(\frac{2\rho g \alpha}{9\eta}\right)^{1/2}\left[\left(R_0^3 + \frac{27\eta k}{2\rho g \alpha} h\right)^{1/2} - R_0^{3/2}\right] \tag{16}$$

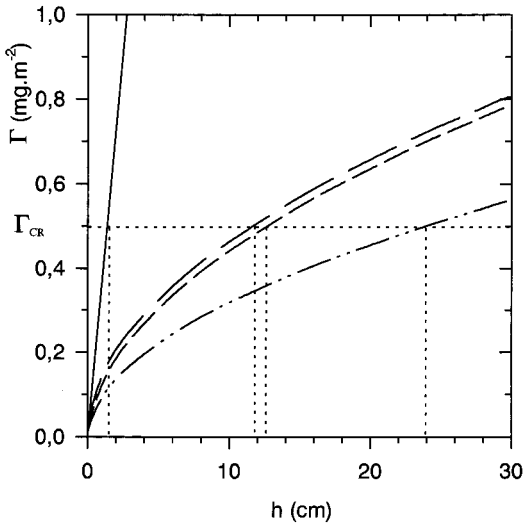

Figure 8. $\Gamma(h)$ from relation (16), with $c_0 = 4.3$ mg/L, $k = 100$ μm/s, and $R_0 = 50$ μm (– – –); $k = 100$ μm/s and $R_0 = 20$ μm (— —); $k = 200$ μm/s and $R_0 = 50$ μm (– - - –), compared with $\Gamma(h)$ for a bubble of fixed radius $R = 50$ μm (—).

By using known values of ρ and η in champagne, the intermediate value of 0.75 for α, the diffusion coefficient of BSA, $D = 6.7 \times 10^{-11}$ m^2 s^{-1},[26] and $\lambda = 0.35$,[25] we suggest an estimation of the surface-active materials surface concentration $\Gamma(h)$ on the ascending bubble

$$\Gamma(h) \approx (2 \times 10^{-3})\frac{c_0}{k}[(R_0^3 + (3 \times 10^{-6})kh)^{1/2} - R_0^{3/2}] \tag{17}$$

Let us now have a closer look at the relative influence of each pertinent parameter c_0, R_0, and k on $\Gamma(h)$.

$\Gamma(h)$ is directly proportional to the bulk concentration of contaminants c_0.

For $c_0 = 4.3$ mg/L, and a typical value of $k = 100$ μm s^{-1},[8] we have plotted in Figure 8 $\Gamma(h)$ for two limiting values of R_0, 20 and 50 μm, respectively, which is the order of magnitude of the bubble radius at detachment in real conditions.[8] It appears clearly that R_0 has a negligible effect on $\Gamma(h)$.

We also have plotted in Figure 8 $\Gamma(h)$ for a bubble of fixed radius $R = 50$ μm and for two expanding bubbles with different growth rates k corresponding to those observed in real conditions.[8] Contrary to its radius at detachment R_0, the bubble growth rate k affects drastically its surface state. k is responsible for the dilution effect of the adsorbed materials. The bubble area increases all the more quickly as k is high. As a result, the traveled distance needed to reach the critical concentration Γ_{CR} is all the more long as k is high, as shown in Figure 8.

Moreover, it appears clearly from Figure 8 that distances needed to reach the critical concentration Γ_{CR} are on the order of 10−30 cm, depending on values of the growth rate k. It is well above traveled distances in real conditions, which means that distances investigated in our experiments ($h \approx 2$−3 cm) are too short to completely rigidify the bubble interface with surface-active compounds. The

(24) Yang, S.-M.; Han, S. P.; Hong, J. J. *J. Colloid Interface Sci.* **1995**, *169*, 125.

(25) Ybert, C. Stabilisation des mousses aqueuses par des protéines. Thesis, Université Louis Pasteur, Strasbourg, France 1998.

(26) Shen, J. J. S.; Probstein, R. F. *Ind. Eng. Chem. Fundam.* **1977**, *16*, 459.

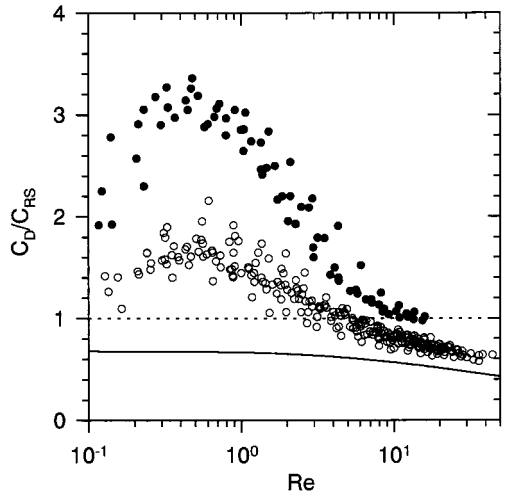

Figure 9. Ratio of the experimental drag coefficient to the drag coefficient of a rigid sphere C_D/C_{RS} as a function of the Reynolds number (Re): champagne bubbles (○), beer bubbles (●); rigid sphere limit (- - -), fluid sphere limit $C_{FS}/C_{RS} = (2/3)[(1 + 0.15Re^{0.5})/3(1 + 0.15Re^{0.687})]$ (—).

semiempirical model of surface-active materials adsorption (eq 16) is therefore compatible with our experimental results.

3.5. Comparison between Champagne and Beer Bubbles. To compare the drag coefficient experienced by bubbles during ascent, with the one experienced by a rigid sphere, we have plotted in Figure 9 the ratio C_D/C_{RS} vs Re during ascent for champagne and beer bubbles. It is possible to distinguish two different regimes during the bubble rise: A first stage attributed to both inertial and wall effects, where $C_D/C_{RS} > 1$, followed by a quasi stationary stage during which the bubble surface state appears constant but nevertheless rather different from champagne to beer. As previously observed, from a traveled distance $h \approx 1$ cm, champagne bubbles behave as partially rigidified spheres ($C_D/C_{RS} < 1$), whereas in beer C_D/C_{RS} appears bounded by the rigid sphere limit (for the traveled distances investigated in our experiments). Shafer and Zare[27] reported, in a previous study of bubble ascent in a glass of beer, that the bubble was hydrodynamically equivalent to a rigid sphere. Thus, all along the rise, the ratio C_D/C_{RS} remains higher for beer bubbles than for champagne bubbles. The drag force exerted on a beer bubble is therefore clearly higher than the one exerted on a champagne bubble. There are three main differences between champagne and beer which may affect the rise of bubbles:

(i) Beer contains much more proteins (122 ± 2 mg/L BSA) than champagne (4.3 ± 0.5 mg/L BSA).

(ii) The dissolved gas content is approximately three times lower in beer than in champagne.

(iii) The ethanol content is higher in champagne (12.2%) than in beer (6.7%).

Since beer contains approximately 30 times more surface-active materials likely to be adsorbed at the bubble interface than champagne, the higher drag coefficient in beer is mainly due to an increase of the amount of contaminants collected during ascent. Furthermore, because the gas content is lower in beer, growth rates k of beer bubbles are lower than those of champagne.[8,27] As a result, the dilution effect due to k is too weak to avoid the rigidification of the bubble interface in beer. Moreover, previous studies demonstrated that properties of adsorption layers are very dependent on the alcohol content.[28−31] As a result, the ethanol also probably affects the bubble rise. Experiments are now conducted along that line.

Acknowledgment. Thanks are due to the Europôl'Agro institute and the "Association Recherche Œnologie Champagne-Université" for financial support, to the Verrerie Cristal d'Arques and Champagne Pommery for supplying glasses and wines, and to Catherine Colin and Jean-Marc di Meglio for valuable discussions.

Notation

c_0	concentration of the surface-active compound in the bulk, mg m^{-3}
C_{AM}	added-mass coefficient
C_D	drag coefficient
C_{FS}	drag coefficient experienced by a fluid sphere
C_{RS}	drag coefficient experienced by a rigid sphere
d	distance from the center of the bubble to the glass wall, m
D	diffusion coefficient of the surface-active compound, m^2 s^{-1}
f	frequency of bubble formation, Hz
F_{AM}	added-mass force, N
F_B	buoyancy, N
F_D	drag force, N
g	acceleration due to gravity, m s^{-2}
h	traveled distance from the nucleation site, m
k	bubble growth rate dR/dt, m s^{-1}
M	Morton number
n	index affected to a bubble of a bubble train
R	bubble radius, m
R_0	bubble radius at detachment, m
Re	Reynolds number
t	time, s
T	period of bubble formation, s
U	bubble velocity, m s^{-1}
U_{FS}	velocity of a fluid sphere, m s^{-1}
U_{LEV}	velocity derived by Levich, m s^{-1}
U_{RS}	velocity of a rigid sphere, m s^{-1}
U_{ST}	Stokes velocity, m s^{-1}
U_∞	velocity in an infinite medium, m s^{-1}

Greek Letters

α	ratio of the experimental bubble velocity to the Stokes velocity
Γ	surface concentration of contaminants, mg m^{-2}
Γ_{CR}	critical surface concentration needed to completely rigidify the bubble interface; (in BSA solutions, Ybert and di Meglio[12] determined that $\Gamma_{CR} = 0.5$ mg m^{-2})
λ	numerical pre-factor in eq 13
η	fluid dynamic viscosity, kg m^{-1} s^{-1}
ν	fluid kinematic viscosity ($\nu = \eta/\rho$), m^2 s^{-1}
ρ	fluid density, kg m^{-3}
σ	liquid surface tension, N m^{-1}
χ	ellipticity of the bubble, ratio of the longer to the smaller axis

LA990653X

(27) Shafer, N. E.; Zare, R. N. *Phys. Today* **1991**, *44*, 48.

(28) Dickinson, E.; Woskett, C. M. *Food Hydrocolloids* **1988**, *2*, 187.

(29) Ahmed, M.; Dickinson, E. *Colloids Surf.* **1990**, *47*, 353.

(30) Dussaud, A.; Han, G. B.; Ter-Minassian-Saraga, L.; Vignes-Adler, M. *J. Colloid Interface Sci.* **1994**, *167*, 247.

(31) Puff, N.; Cagna, A.; Aguié-Beghin, V.; Douillard, R. *J. Colloid Interface Sci.* **1998**, *208*, 405.